NASA/TM—2018-220033

Heat Transfer Measurements on the Endwall of a Variable Speed Power Turbine Blade Cascade

Douglas R. Thurman
U.S. Army Research Laboratory, Glenn Research Center, Cleveland, Ohio

Philip E. Poinsatte
Glenn Research Center, Cleveland, Ohio

Paul W. Giel
Vantage Partners, LLC, Brook Park, Ohio

Barbara L. Lucci
Glenn Research Center, Cleveland, Ohio

December 2018

NASA STI Program . . . in Profile

Since its founding, NASA has been dedicated to the advancement of aeronautics and space science. The NASA Scientific and Technical Information (STI) Program plays a key part in helping NASA maintain this important role.

The NASA STI Program operates under the auspices of the Agency Chief Information Officer. It collects, organizes, provides for archiving, and disseminates NASA's STI. The NASA STI Program provides access to the NASA Technical Report Server—Registered (NTRS Reg) and NASA Technical Report Server—Public (NTRS) thus providing one of the largest collections of aeronautical and space science STI in the world. Results are published in both non-NASA channels and by NASA in the NASA STI Report Series, which includes the following report types:

- TECHNICAL PUBLICATION. Reports of completed research or a major significant phase of research that present the results of NASA programs and include extensive data or theoretical analysis. Includes compilations of significant scientific and technical data and information deemed to be of continuing reference value. NASA counter-part of peer-reviewed formal professional papers, but has less stringent limitations on manuscript length and extent of graphic presentations.

- TECHNICAL MEMORANDUM. Scientific and technical findings that are preliminary or of specialized interest, e.g., "quick-release" reports, working papers, and bibliographies that contain minimal annotation. Does not contain extensive analysis.

- CONTRACTOR REPORT. Scientific and technical findings by NASA-sponsored contractors and grantees.

- CONFERENCE PUBLICATION. Collected papers from scientific and technical conferences, symposia, seminars, or other meetings sponsored or co-sponsored by NASA.

- SPECIAL PUBLICATION. Scientific, technical, or historical information from NASA programs, projects, and missions, often concerned with subjects having substantial public interest.

- TECHNICAL TRANSLATION. English-language translations of foreign scientific and technical material pertinent to NASA's mission.

For more information about the NASA STI program, see the following:

- Access the NASA STI program home page at http://www.sti.nasa.gov

- E-mail your question to help@sti.nasa.gov

- Fax your question to the NASA STI Information Desk at 757-864-6500

- Telephone the NASA STI Information Desk at 757-864-9658

- Write to:
  NASA STI Program
  Mail Stop 148
  NASA Langley Research Center
  Hampton, VA 23681-2199

NASA/TM—2018-220033

Heat Transfer Measurements on the Endwall of a Variable Speed Power Turbine Blade Cascade

Douglas R. Thurman
U.S. Army Research Laboratory, Glenn Research Center, Cleveland, Ohio

Philip E. Poinsatte
Glenn Research Center, Cleveland, Ohio

Paul W. Giel
Vantage Partners, LLC, Brook Park, Ohio

Barbara L. Lucci
Glenn Research Center, Cleveland, Ohio

Prepared for the
74th Annual Forum and Technology Display (Forum 74)
sponsored by the American Helicopter Society (AHS) International
Phoenix, Arizona, May 14–17, 2018

National Aeronautics and
Space Administration

Glenn Research Center
Cleveland, Ohio 44135

December 2018

Acknowledgments

This research was sponsored by NASA's Revolutionary Vertical Lift Technologies Project under the Aeronautics Research Mission Directorate.

This work was sponsored by the Advanced Air Vehicle Program at the NASA Glenn Research Center

Level of Review: This material has been technically reviewed by technical management.

Available from

NASA STI Program
Mail Stop 148
NASA Langley Research Center
Hampton, VA 23681-2199

National Technical Information Service
5285 Port Royal Road
Springfield, VA 22161
703-605-6000

This report is available in electronic form at http://www.sti.nasa.gov/ and http://ntrs.nasa.gov/

Heat Transfer Measurements on the Endwall of a Variable Speed Power Turbine Blade Cascade

Douglas R. Thurman
U.S. Army Research Laboratory
Glenn Research Center
Cleveland, Ohio 44135

Philip E. Poinsatte
National Aeronautics and Space Administration
Glenn Research Center
Cleveland, Ohio 44135

Paul W. Giel
Vantage Partners, LLC
Brook Park, Ohio 44142

Barbara L. Lucci
National Aeronautics and Space Administration
Glenn Research Center
Cleveland, Ohio 44135

Summary

Heat transfer measurements were obtained on the planar endwall of a two-dimensional (2D) section of a variable speed power turbine (VSPT) rotor blade in a linear cascade. Infrared (IR) thermography was used to determine the endwall heat transfer distribution. Changes in the local heat transfer rates with Reynolds number (Re) were used to identify the laminar, turbulent, and transitional flow regimes as well as to determine regions of flow separation. Steady-state data were obtained for six incidence angles, ranging from +15.8° to –51.0°, and at five flow conditions for each angle. Reynolds numbers were varied over an order of magnitude while two exit Mach number (M) conditions were examined in order to accommodate the facility operating envelope.

Introduction

Future vertical lift vehicles that can have both vertical takeoff and 0.5 Mach (M) cruise capability will require enabling technologies such as variable speed power turbines (VSPT) or multiple gear ratios (Refs. 1 and 2) in order to maintain high propulsive efficiency. While a conventional method for reducing turbine speed is through gearing, future aircraft may require up to a 50-percent reduction in the main rotor speed during cruise at nearly constant engine corrected flow rates. As a result of this change in rotor speed, the power turbine blades and vanes will see large variations in incidence flow angle. Technologies using incident-tolerant blading can optimize propulsive efficiency by allowing the power turbine to change shaft speed while minimizing weight and fuel consumption. A VSPT must overcome these large incidence flow angle variations at high work factors and low Reynolds numbers, Re, over a wide operational speed range in order to be viable.

Several studies have addressed some of the challenges that are relevant to variable speed turbines. Welch et al. (Ref. 2) provided details of the VSPT technology and the followup technology transitions. Johnson et al. (Ref. 3) and Acree et al. (Ref. 4) described the benefits and challenges of vertical lift and 0.5 M cruise-capable rotary-wing vehicles such as NASA's Large Civil Tilt-Rotor (LCTR) concept vehicle. The LCTR was the reference vehicle used as the baseline for several aerodynamic studies performed by NASA and the U.S. Army Research Laboratory. Experimental VSPT studies have been reported in References 5 to 7, detailing aerodynamic performance through five-hole probe surveys at various Reynolds numbers and incidence angles, blade loading, and loss buckets. Computational fluid dynamics (CFD) simulations will be used to design and analyze future VSPT blading. The accuracy of these simulations is highly dependent on their ability to predict laminar, turbulent, and transitional flow regimes, particularly as Reynolds numbers decrease at altitude cruise conditions where separation-induced losses can become prevalent. Low-turbulence experimental data within VSPT blade rows can prove to be challenging test cases for CFD code and model improvement. The experimental determination of

the local laminar, turbulent, and transitional flow regimes as well as the identification of separated flow regimes is critical to the improvement of CFD predictive capability needed to optimize future VSPT blade designs.

The objective of the present study is to advance the understanding of the aerodynamic effects of large-incidence angle and Reynolds number variations in order to address key VSPT challenges. One of those challenges is to improve the computational modeling of complicated flows such as those seen in a VSPT blade row with a wide range of incidence angles and flow rates. In the present study, sections of the planar endwall in a linear cascade were heated electrically and endwall heat transfer distributions were determined by using infrared (IR) thermography. Changes in the local heat transfer rates with Reynolds number were then used to identify the laminar, turbulent, and transitional flow regimes as well as to determine regions of flow separation. The heat transfer measurements in this study were not meant to be used to determine cooling requirements, but rather to be used as a method to visualize flow transition and separation on the endwall surface. A range of Reynolds numbers spanning an order of magnitude of the baseline flow condition were investigated at several incidence angles similar to studies described in References 5 to 7. The endwall data, along with the blade surface heat transfer data currently being acquired, will provide beneficial information for CFD code and turbulence model improvement and help optimize future incident tolerant blade designs.

Description of Experiment

Heat transfer measurements on the endwall of the two-dimensional (2D) VSPT blade section were conducted in the Transonic Turbine Blade Cascade Facility at the NASA Glenn Research Center, shown in Figure 1. A description of the facility can be found in Reference 5. The cascade comprises nominally 10 blades that represent a scaled 2D midspan section of the VSPT second-stage rotor, with geometry details described in Reference 8 and summarized in Table I. The facility has the capability to test large-scale models (span of 6 in.) with continuous flow at engine relevant Mach and Reynolds numbers. In addition, the cascade is attached to a wheel that can be rotated to provide incidence angles from +15.8° to –51.0°, as shown in Figure 2; this allows for a wide range of incidence angles to be studied. Table II lists the angles that were examined in this study. Inlet air is supplied by a 40-psig combustion air system, which provides clean, dry ambient temperature air. The air is then passed through a flow conditioner and a contraction section, then into the main test section with upper and lower flow boards, and exhausted through an altitude exhaust system maintained at 2 psia. For the current tests, no inlet turbulence grid was installed, providing low inlet turbulence intensities of 0.8 percent.

At each incidence angle setting from Table II, data were acquired at the five nominal flow conditions listed in Table III. The design pressure ratio of 1.412 was used, which corresponds

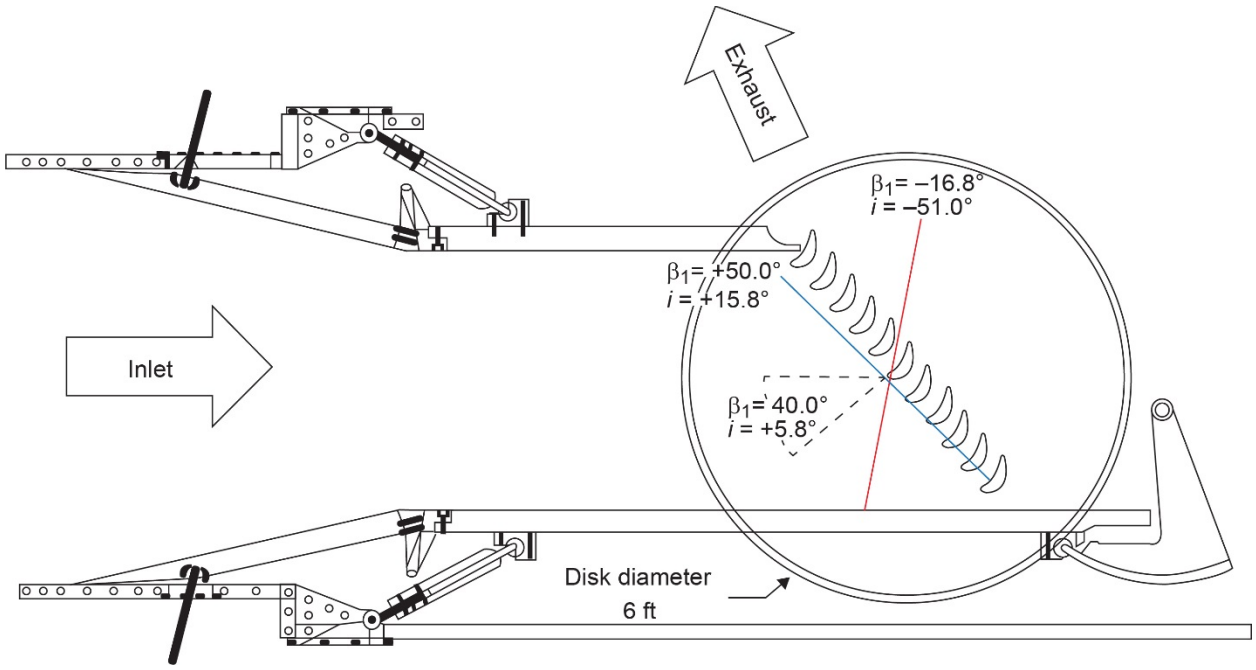

Figure 1.—Transonic turbine blade cascade facility, where i is incidence angle and β is relative flow angle, pitch angle (deg).

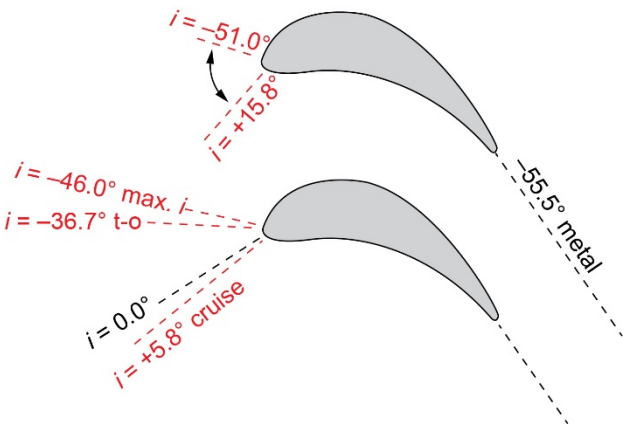

Figure 2.—Incidence angles of VSPT blade, where *i* is incidence angle.

TABLE I.—BLADE PARAMETERS

Axial chord, C_x (in.)	7.109
True chord, in.	7.655
Pitch, *S* (in.)	5.119
Span, *H* (in.)	6.000
Solidity, C_x/S	1.389
Aspect ratio, H/C_x	0.844
Throat dimension, in.	2.868
Stagger angle, deg	20.35
Inlet metal angle, deg	34.2
Uncovered turning, deg	19.47
Exit metal angle, deg	–55.54

TABLE II.—INLET FLOW ANGLES

Incidence angle, *i*	Tunnel inlet angle, β_1	Zw
+15.8°	+50.0°	1.22
+5.8° (cruise)	+40.0°	1.06
–16.1°	+18.1°	0.82
–36.7° (takeoff)	–2.5°	0.65
–46.0° (max. mission)	–11.8°	0.58
–51.0°	–16.8°	0.53

to an exit isentropic Mach number, $M_{2,i}$, of 0.72. The baseline exit Reynolds number, Re_b, based on axial chord length, was determined by finding the lowest Reynolds number at which the tunnel could maintain an exit of 0.72 M, which was found to be 0.53×10^6. Since the lowest Reynolds number of 2.12×10^5 could not be reached at the design exit Mach number due to limitations of the tunnel operating envelope, the Mach number for this case was reduced to 0.35. Additional overlap flow points were tested at $M_{2,i}$ of 0.35 and 0.72 at $1.0 \times Re_b$. Nominal endwall inlet boundary layer thickness ranged from 1.6 in. at the lowest Reynolds number to 1.2 in. at the highest Reynolds number.

TABLE III.—NOMINAL TUNNEL FLOW CONDITIONS[a,b]

Case no.	Exit Reynolds number, $Re_{Cx,2}$	Reynolds number baseline factor	Pressure ratio, *PR*	Exit Mach number, $Ma_{2,i}$
1	0.212×10^6	0.4	1.087	0.35
2	0.530×10^6	1.0	1.087	0.35
3	0.530×10^6	1.0	1.412	0.72
4	1.060×10^6	2.0	1.412	0.72
5	2.120×10^6	4.0	1.412	0.72

[a]Baseline exit Reynolds number, Re_b = 530,000.
[b]Design pressure ratio = 1.412 → $M_{2,i}$ = 0.72.

The instrumented section of the endwall was a foam insert coated with a gelcoat that fit inside an aluminum outer wall. Five heater strips connected in series were attached to the foam endwall section spanning one of the passages between blades 5 and 6 in the cascade, as shown in Figure 3(a). Inconel® (Special Metals Corporation) foil with a thickness of 0.001 in. was attached to the surface with double-sided tape, with the end of each strip tack welded to a copper bus bar. With the five heater strips connected in series, one end each of heater strips 1 and 5 were connected to a direct-current (DC) power supply. The blades on the heated endwall had thin rubber gaskets on their ends to electrically isolate them from the heaters.

The heater power was determined for each individual heater strip through accurate measurements of heater voltage and current. Two thin-film thermocouples were attached to the surface to provide a surface temperature for calibration of the IR thermography images. Two forward-looking infrared (FLIR) cameras were used to acquire temperature data on the endwall, with one camera viewing the upstream portion of the passage and one viewing the downstream portion of the passage through two coated ZnSe IR viewing ports, as shown in Figure 3(b). The endwall was painted flat black to provide an emissivity of approximately 0.96, and a 1- by 1-in. grid of fiducial dots was painted on the surface to assist in correcting any angled or distorted images.

Nusselt numbers were determined using the following equation:

$$\mathrm{Nu} = \frac{h \cdot C_x}{k} = \frac{Q \cdot C_x}{A \cdot k \cdot \Delta T}$$

in which *Q* is the heater strip power, *A* is the total area of each heater strip, C_x is the blade axial chord length, and *k* is the thermal conductivity of the air. The temperature difference ΔT is the difference between the surface temperature from an image acquired with heat applied and the adiabatic surface temperature from an image acquired with no heat applied. The adiabatic surface temperatures were used to account for compressible flow effects. Since the images were taken at angles and the cameras were not completely perpendicular to the surface, the Nusselt

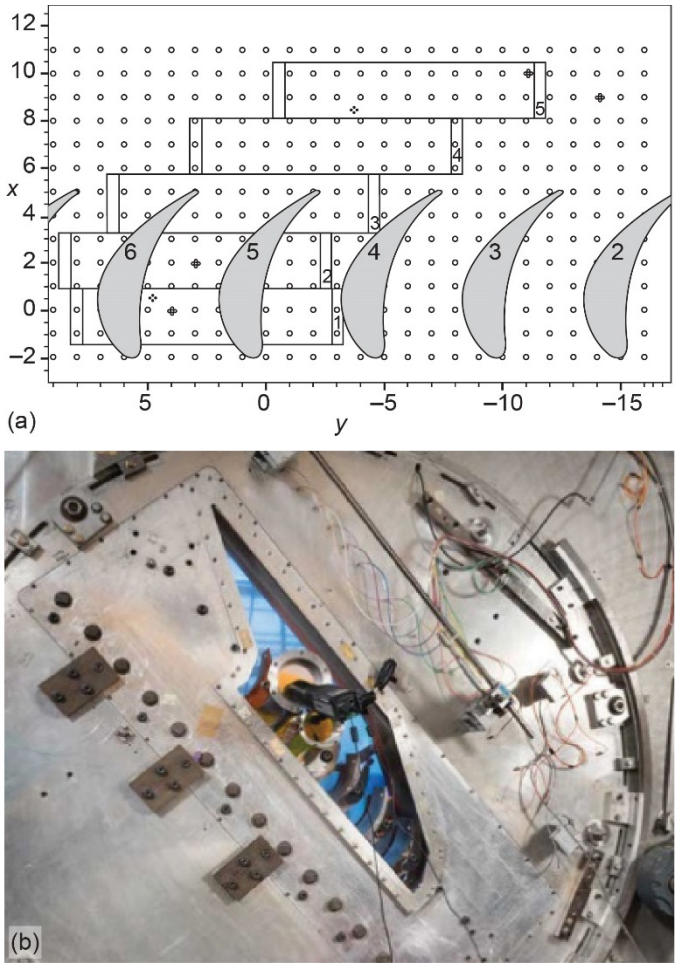

Figure 3.—Endwall test section. (a) Heater strip locations. (b) Infrared window ports and cameras.

images were run through a view correction program and converted to unwrapped Cartesian coordinates.

Experimental Results

Figure 4 and Figure 5 show a composite plot of Nusselt numbers for the five flow conditions at blade incidence angles of +5.8° cruise condition and –36.7° takeoff condition. Note that the scales are not the same and were chosen to bound the minimum and maximum Nusselt numbers for each flow condition. Also, the high-Nu regions near the leading edge of the first heater strip and on the edges of each of the downstream heater strips are a result of the adjacent unheated surfaces. As expected, Figure 4 shows heat transfer rates increase with increasing Reynolds number, and strong secondary flow features are evident. Comparing cases 2 and 3, which have the same Reynolds number of $1.0 \times \mathrm{Re}_b$ but different $\mathrm{M}_{2,i}$, the Nusselt number contours appear to be similar, with a low Nu region near the center of the passage. This is not surprising given that Nusselt number is a stronger function of Reynolds number than of Mach number. As the Reynolds number increases, this low Nu region diminishes; Nu increases as the region of turbulent flow begins to increase in the passage. In addition, the wake behind the trailing edge of the blade appears to be shifted toward the suction surface of the passage. Low Nusselt number regions can be seen near the aft suction surface of the blade, possibly indicating separated flow in the uncovered flow turning region. This corresponds with the secondary flow pattern seen in the previously acquired pressure survey data from Reference 5. Figure 6 shows the pitchwise and spanwise total pressure coefficients at 7-percent axial chord distance downstream of the trailing edge plane of the blade, with y representing the pitchwise direction and z representing the spanwise direction. The small corner vortex seen near the endwall agrees with the location of the wake in the heat transfer data.

Figure 5 shows composite plots at the takeoff blade incidence angle of –36.7°. Again, these plots are not on the same scale and are bounded by the minimum and maximum Nusselt number for each flow condition, and the high-Nu regions near the leading edge of the first heater strip and on the edges of each of the downstream heater strips are a result of the adjacent unheated surfaces. The flow pattern through the passage has changed relative to that seen at the cruise incidence angle, however, there still appears to be a slight separation region near the aft suction surface similar to the cruise angle. This is also seen in the pressure survey data shown in Figure 6. A higher Nu wake can be seen directly behind the blade trailing edge, with a shifted low-Nu region farther downstream. This again corresponds with the secondary flow pattern seen in the previously acquired pressure survey data in Figure 6. Effects of the passage and horseshoe vortices generated from the leading edge of the blade can be seen in the streak of low Nu across the middle of the passage. Because of the lower flow turning, the pressure surface leg of the passage and horseshoe vortex remains closer to the endwall than for the cruise conditions. Cases 2 and 3 are again similar to each other. A small high-Nu region near the midchord of the suction surface is seen in the accelerating region of the passage. This accelerating region increases with increasing Reynolds numbers.

Nusselt number data from six incidence angles at $4.0 \times \mathrm{Re}_b$ are shown in Figure 7. The other flow conditions showed similar trends and are not included here for brevity. Starting with $i = +15.8°$, the separation region on the aft suction surface can be seen to get smaller as incidence angle decreases. The low Nusselt number streak near midpassage is seen again at the extreme negative incidence angles. Relatively high heat transfer rates are present on the near trailing edge portion of the pressure surface for the negative incidences, which are most likely due to transition and not caused by reattachment.

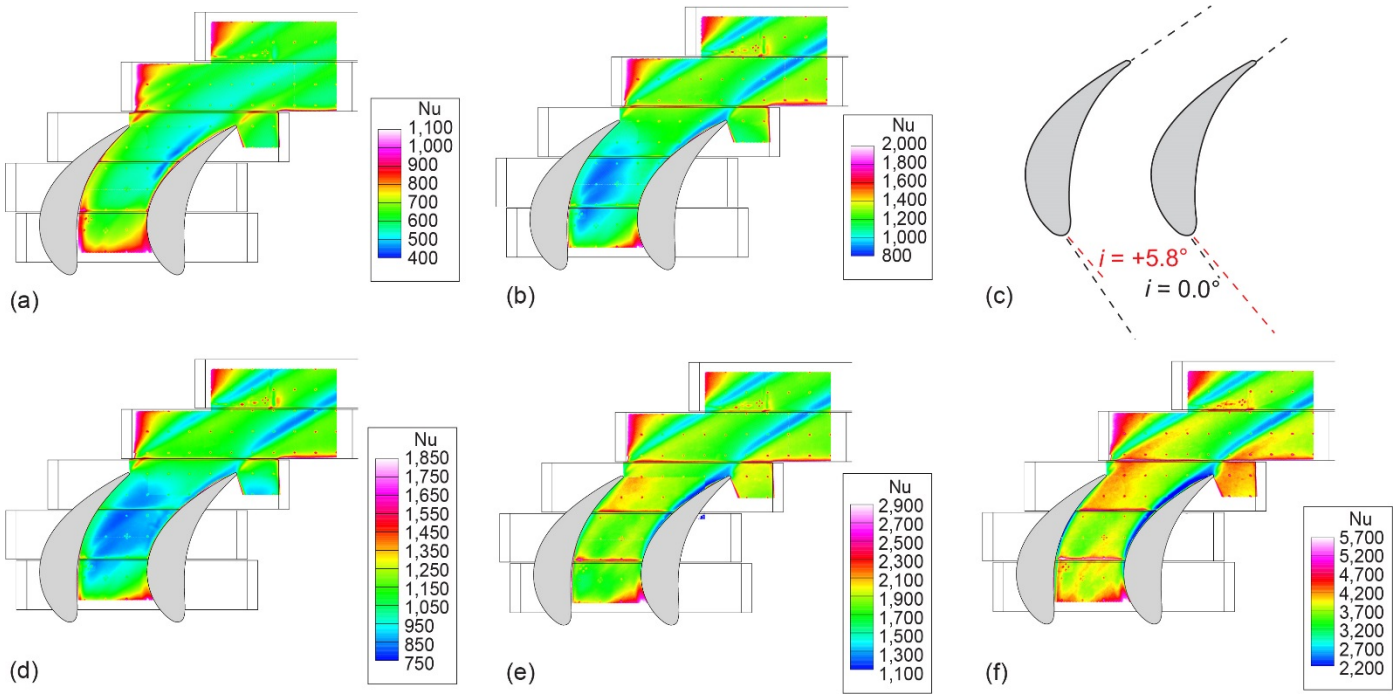

Figure 4.—Endwall Nusselt number (Nu) at cruise condition, where incidence angle, i, is +5.8, M is Mach number, Re is Reynolds number, and Re_b is baseline exit Reynolds number. (a) Case 1, where M = 0.35 and Re = 0.4 × Re_b. (b) Case 2, where M = 0.35 and Re = 1.0 × Re_b. (c) Incidence angles of variable speed power turbine blade. (d) Case 3, where M = 0.72 and Re = 1.0 × Re_b. (e) Case 4, where M = 0.72 and Re = 2.0 × Re_b. (f) Case 5, where M = 0.72 and Re = 4.0 × Re_b.

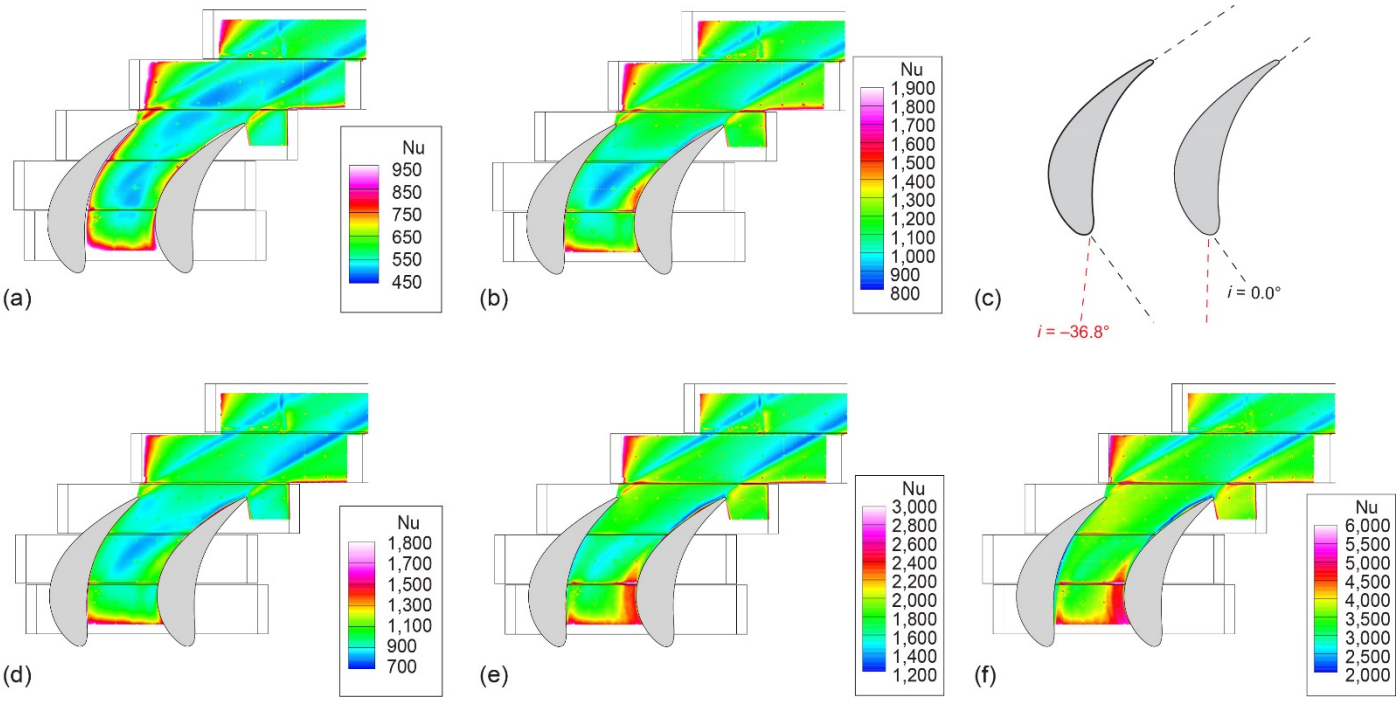

Figure 5.—Endwall Nusselt number (Nu) at takeoff where incidence angle (i) is –36.7°, M is Mach number, Re is Reynolds number, and Re_b is baseline exit Reynolds number. (a) Case 1, where M = 0.35 and Re = 0.4 × Re_b. (b) Case 2, where M = 0.35 and Re = 1.0 × Re_b. (c) Incidence angles of variable speed power turbine blade. (d) Case 3, where M = 0.72 and Re = 1.0 × Re_b. (e) Case 4, where M = 0.72 and Re = 2.0 × Re_b. (f) Case 5, where M = 0.72 and Re = 4.0 × Re_b.

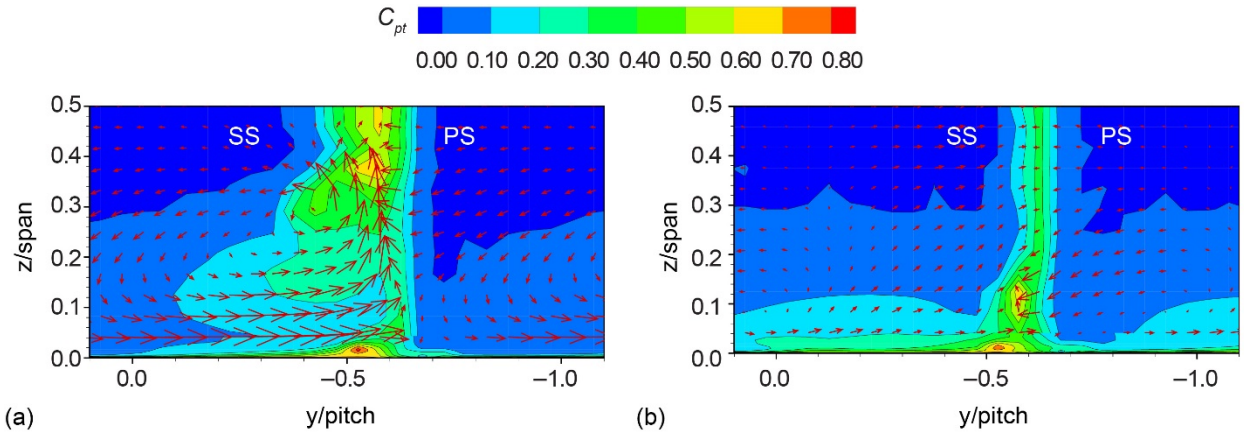

Figure 6.—Total pressure coefficient contours and secondary flow vectors over one blade passage downstream of blade (Ref. 5), where C_{pt} is total-pressure coefficient, i is incidence angle, PS is pressure surface, SS is suction surface. (a) i = +5.8°. (b) i = –36.7°.

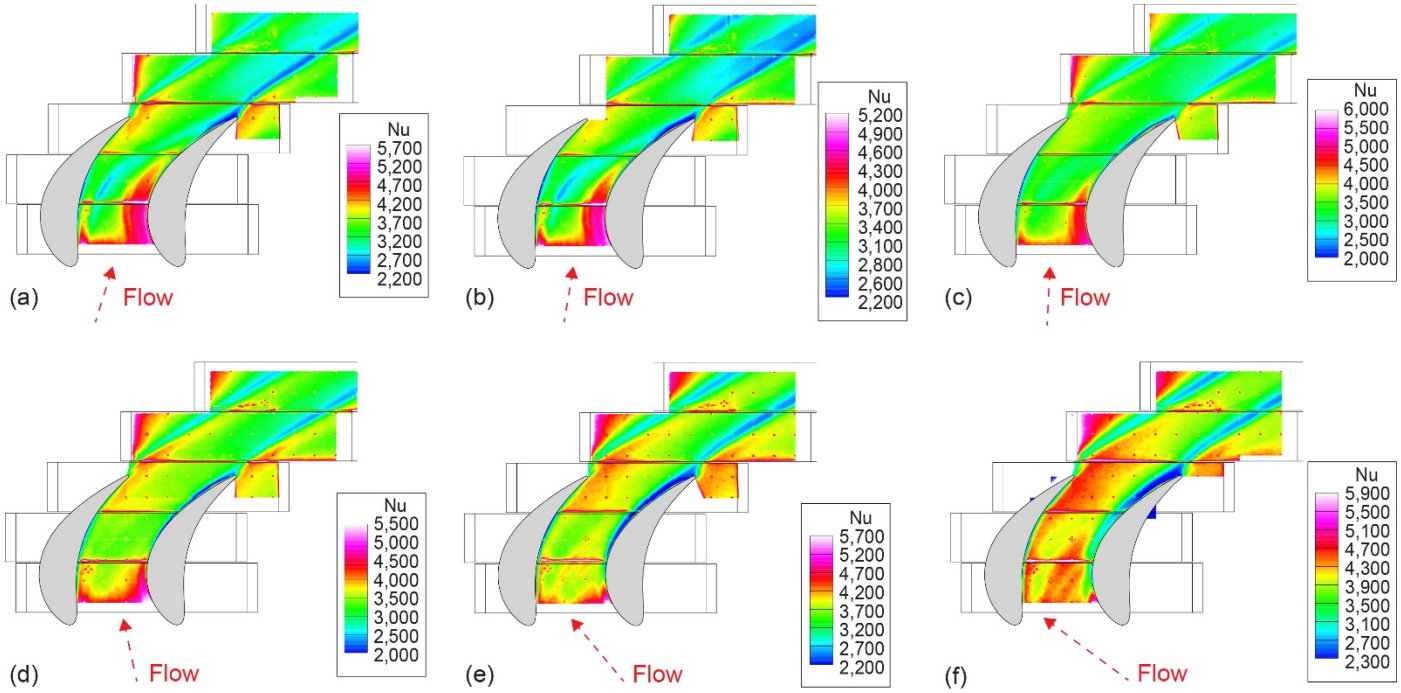

Figure 7.—Endwall Nusselt number (Nu) at 4.0 × Re_b for case 5, where i is incidence angle, M is Mach number, and Re_b is baseline exit Reynolds number. (a) M = 0.72 and i = –51.0°. (b) M = 0.72 and i = –46.0°. (c) M = 0.72 and i = –36.7°. (d) M = 0.72 and i = –16.1°. (e) M = 0.72 and i = +5.8°. (f) M = 0.72 and i = +15.8°.

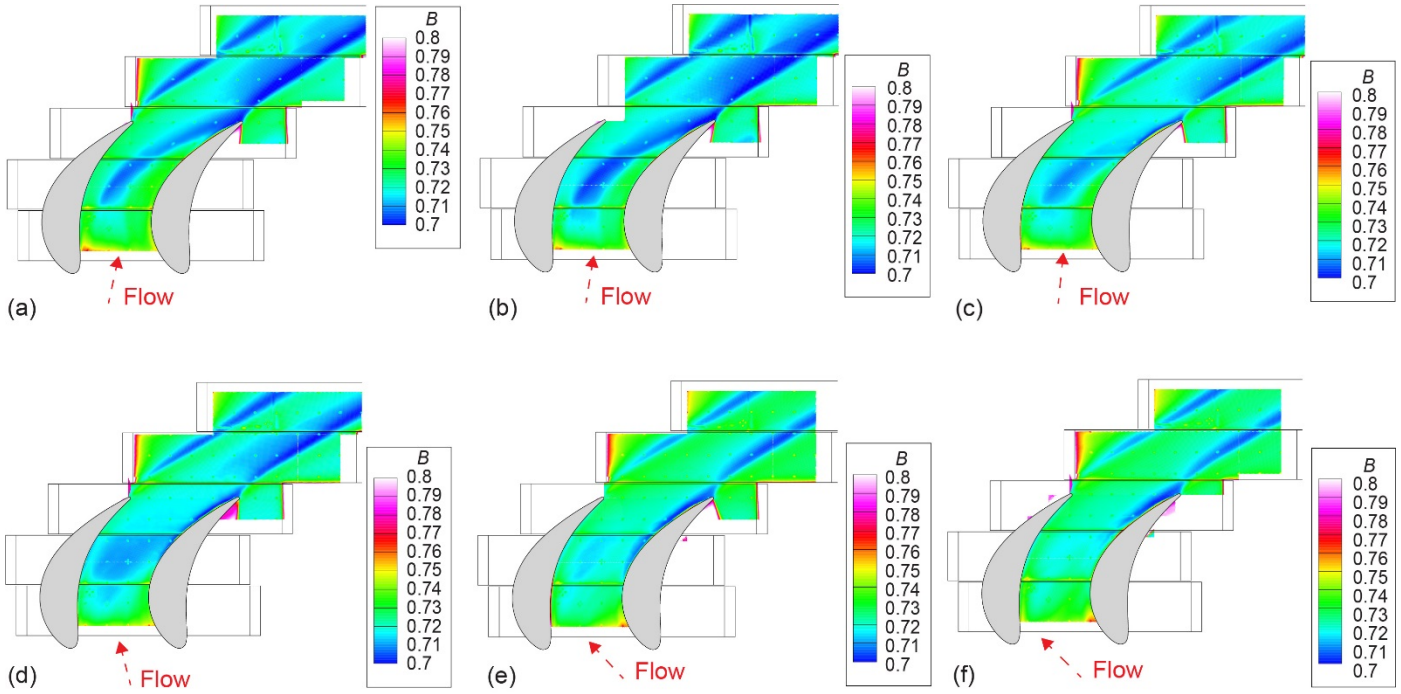

Figure 8.—Values of the exponent, *B*, of the Nusselt-Reynolds correlation Nu = 0.837 × Re^B, where *i* is incidence angle and Re^B is Reynolds number with exponent value. (a) *i* = –51.0°. (b) *i* = –46.0°. (c) *i* = –36.7°. (d) *i* = –16.1°. (e) *i* = +5.8°. (f) *i* = +15.8°.

Flow transition was also investigated by comparing the Nusselt-Reynolds number correlation values for the different flow conditions, where Nu = $A \times Re^B$. While this correlation was developed for flow over a flat plate, it is still useful for determining where flow transitions from laminar to turbulent on the endwall. Plotting local values of the exponent *B* calculated from multiple flow conditions gives an indication of the state of the local boundary layer as the flow transitions from one condition to another. For a flat plate, a value for *B* of 0.5 indicates laminar flow, and a value of 0.8 indicates turbulent flow. Guzovic, Matijasevic, and Rusevljan (Ref. 9) determined a generalized statistical correlation for a cascade endwall for flow conditions ranging from laminar through turbulent, yielding *A* = 0.0837 and *B* = 0.7494. The current data from all flow cases at each incidence angle was fit to this form. The coefficient *A* was forced to 0.0837, and *B* was determined locally by a least squares data fit for all five flow cases and is shown in Figure 8. The results show exponent values that match Guzovic's correlation fairly well with exponent values near 0.73. The higher Reynolds number cases are expected to be mostly turbulent, and Figure 8 generally indicates a mostly turbulent flow situation. There may be some indication of laminar or possibly separated flow near the suction-side trailing edge corner vortex region, where lower values of *B* are located, as well as the passage vortex at the more negative incidence angles. This is also similar to what was seen in the Nusselt number distributions of Figure 7.

While analysis of Reference 9 provides an overall average indication of flow status, the local flow status can better be evaluated by comparing Nusselt number changes for two Reynolds cases to determine if any regions of laminar flow are evident. A ratio of the Nusselt correlation based on two flow conditions can be used to determine the exponent *B*:

$$\frac{Nu_2}{Nu_1} = \left(\frac{Re_2}{Re_1}\right)^B \rightarrow B = \frac{\ln\left(Nu_2 / Nu_1\right)}{\ln\left(Re_2 / Re_1\right)}$$

Figure 9(a) shows values of the exponent *B* for the ratios of case 1 (M = 0.35 and Re = 0.4 × Re_b) and case 2 (M = 0.35 and Re = 1.0 × Re_b) for the cruise angle. Similarly, Figure 9(b) shows values of *B* for the ratios of case 3 (M = 0.72 and Re = 1.0 × Re_b) and case 5 (M = 0.72 and Re = 4.0 × Re_b) at the cruise angle. Figure 9(a) seems to show areas of laminar flow transitioning to turbulent flow. The inlet endwall boundary layer is fully turbulent, so it is possible that at lower Reynolds numbers, the acceleration through the passage relaminarized the flow, especially near the pressure surface. This is consistent with the relaminarization reported by Giel et al. (Ref. 10) for flow on the pressure surface of a cascade blade, even at very high inlet turbulence intensity. Because the acceleration parameter is proportional to $1/(\rho \cdot U^2)$, relaminarization is more likely at lower Reynolds numbers where density is lower and near the pressure

surface where the velocity is lower. Additionally, lower values of *B* can be seen near the aft suction surface corner vortex region. The exponent values greater than 0.8 in Figure 9(b) seem to indicate turbulent flow throughout most of the endwall passage, with the exception being near the suction surface trailing edge. Note that in the midchord-midpitch region, values of *B* as high as 1.25 are seen, which is much higher than the typical turbulent flat plate values of 0.8; this is most likely due to the strong secondary flows in the passage augmenting the heat transfer to levels higher than those associated with typical turbulence. Figure 9(c) and (d) show similar results for the case 1 and case 2 as well as the case 3 and case 5 correlations at the takeoff angle. Changing incidence angle affects the main and secondary flow features, and thus the general shape of the endwall heat transfer distribution is different. Similar to the lower Reynolds number cases at cruise angle, there are regions of lower heat transfer (lower values of *B*) that would indicate laminar flow, particularly near the pressure surface where relaminarization would be more likely. The higher Reynolds cases again indicate a more turbulent flow, with a few regions of very high heat transfer where high acceleration occurs along the suction surface. Comparing Figure 9(b) and (d), it is noted that secondary flow augmentation levels are significantly lower at the takeoff incidence of Figure 9(d) due to greatly reduced levels of secondary flow resulting from reduced overall flow turning. Note, however, that the trailing edge suction surface still shows some signs of laminar flow.

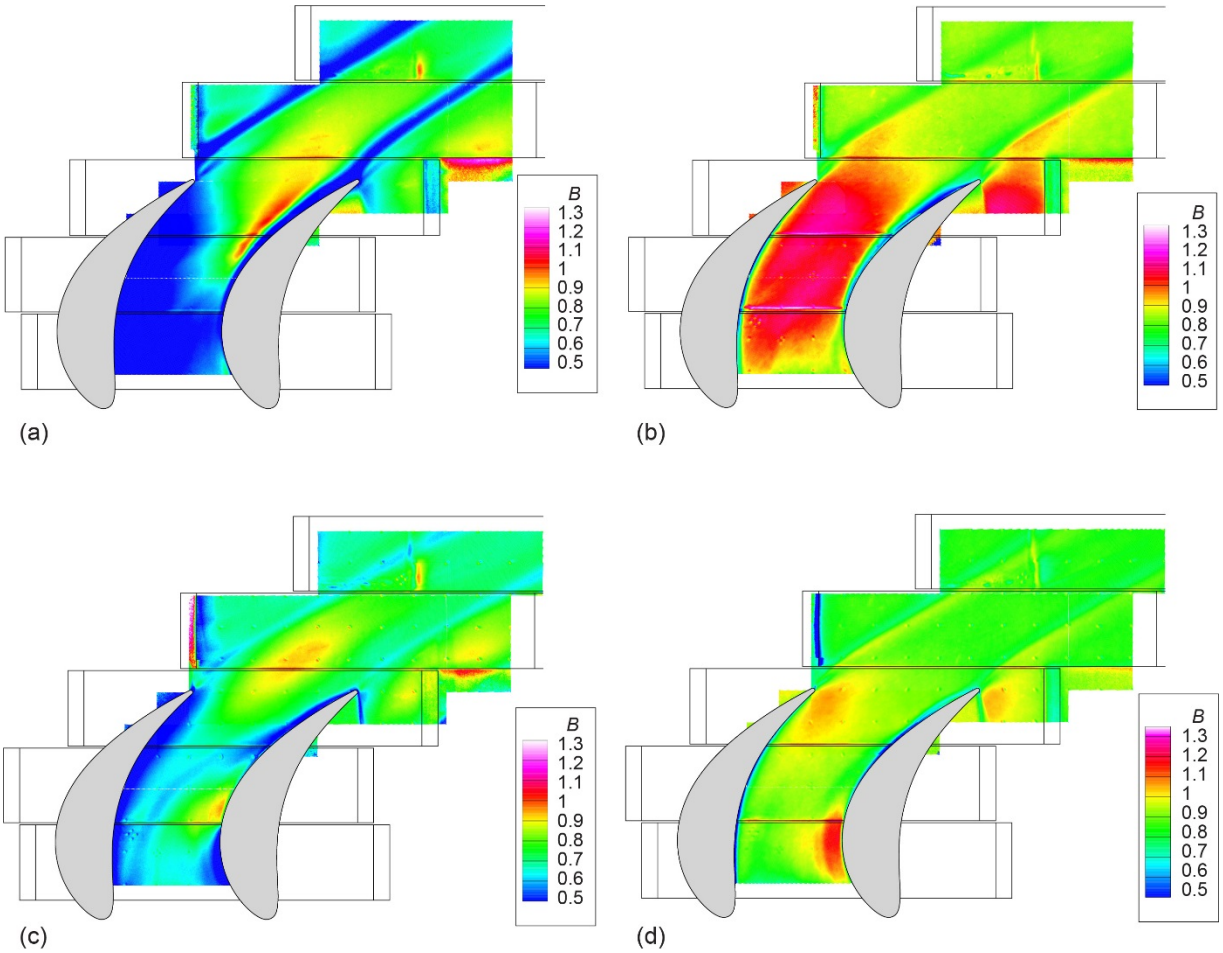

Figure 9.—Values of the exponent *B* from ratio of Nusselt-Reynolds correlations, where *i* is incidence angle, M is Mach number, Re is Reynolds number, and Re_b is baseline exit Reynolds number. (a) At cruise condition, where M = 0.35, Re = 0.4 × Re_b and 1.0 × Re_b, and *i* = +5.8°. (b) At cruise condition, where M = 0.72, Re = 1.0 × Re_b and 4.0 × Re_b, and *i* = +5.8°. (c) At takeoff condition, where M = 0.35, Re = 0.4 × Re_b and 1.0 × Re_b, and *I* = –36.7°. (d) At takeoff condition, where M = 0.72, Re = 1.0 × Re_b and 4.0 × Re_b, and *i* = –36.7°.

Conclusions

The effects of flow transition and separation were investigated over large variations in incidence angle and Reynolds number by using infrared (IR) thermography on the endwall of a variable speed power turbine (VSPT) cascade at low turbulence intensity. Heat transfer measurements on the endwall were acquired for several incidence angles and flow rates, showing regions where separated flow occurred along the endwall surface. A Nusselt-Reynolds number correlation provided insight for where transition from laminar to turbulent flow may occur along the passage between blades. Additional heat transfer tests are currently being investigated on the surface of an instrumented blade to complement the endwall data presented in this study.

Appendix—Nomenclature

2D	two-dimensional
CFD	computational fluid dynamics
DC	direct current
FLIR	forward-looking infrared
IR	infrared
LCTR	Large Civil Tilt Rotor
PS	pressure surface
SS	suction surface
VSPT	variable speed power turbine

Symbols

A	total area of each heater strip
B	exponent value
C_{pt}	total-pressure coefficient, $C_{pt} = (P_{t,1}–P_t)/(P_{t,1}–P_2)$
C_x	blade axial chord length
C_x/S	solidity
H	span
H/C_x	aspect ratio
h	heat transfer coefficient
i	incidence angle, $i = \beta_1$ – inlet metal angle (34.2°)
k	thermal conductivity of air
M	Mach number
$M_{2,i}$	exit isentropic Mach number
$M_{a2,i}$	exit Mach number
Nu	Nusselt number
PR	pressure ratio, $PR = P_{t,1}/ P_2$
P	area-averaged static-pressure
P_t	area-averaged total-pressure
Q	heater strip power
Re	Reynolds number, $\mathrm{Re} = \rho U C_x/\mu$
Re^B	Reynolds number with exponent value
Re_b	baseline exit Reynolds number, $\mathrm{Re}_b = 5.30\times10^5$
$\mathrm{Re}_{Cx,2}$	exit Reynolds number
S	blade pitch, in.
T	temperature
U	total mean velocity
x	chordwise (axial) coordinate, in.
y	pitchwise (tangential) coordinate, in.
z	spanwise coordinate, in.
Zw	Zweifel coefficient, $\mathrm{Zw} = \frac{2S}{C_x}\cos^2\beta_2\left(\tan\beta_1 - \tan\beta_2\right)$
β	relative flow angle, pitch angle (deg), $\beta = \tan^{-1}(U_y/U_x)$
μ	dynamic viscosity
ρ	density

Subscripts

1	cascade inlet value
2	cascade exit value
i	isentropic value
t	total condition

References

1. D′Angelo, Martin: Wide Speed Range Turboshaft Study. NASA CR–198380, 1995. http://ntrs.nasa.gov
2. Welch, Gerard E.: Assessment of Aerodynamic Challenges of a Variable-Speed Power Turbine for Large Civil Tilt-Rotor Application. NASA/TM—2010-216758, 2010. http://ntrs.nasa.gov
3. Johnson, Wayne; Yamauchi, Gloria K.; and Watts, Michael E.: NASA Heavy Lift Rotorcraft Systems Investigation. NASA/TP—2005-213467, 2005. http://ntrs.nasa.gov
4. Acree, C.W., Jr.; Hyeonsoo, Yeo; and Sinsay, Jeffrey D.: Performance Optimization of the NASA Large Civil Tiltrotor. NASA/TM—2008-215359, 2008. http://ntrs.nasa.gov
5. Flegel-McVetta, Ashlie B.; Giel, Paul W.; and Welch, Gerard E.: Aerodynamic Measurements of a Variable-Speed Power-Turbine Blade Section in a Transonic Turbine Cascade at Low Inlet Turbulence. NASA/TM—2013-218069 (GT2013–94695), 2013. http://ntrs.nasa.gov
6. Flegel, Ashlie B.; Giel, Paul W.; and Welch, Gerard E.: Aerodynamic Effects of High Turbulence Intensity on a Variable-Speed Power-Turbine Blade With Large Incidence and Reynolds Number Variations. AIAA 2014–3933 (NASA/TM—2014-218137), 2014. http://ntrs.nasa.gov
7. Flegel, A., et al.: Complementary Aerodynamic Performance Datasets for Variable Speed Power Turbine Blade Section From Two Independent Transonic Turbine Cascades. ISABE–2015–20163, 2015.
8. Ford, A., et al.: Design Optimization of Incidence-Tolerant Blading Relevant to Large Civil Tilt-Rotor Power Turbine Applications. NASA/CR—2012-217016, 2012. Available from the NASA STI Program.
9. Guzovic, Zvonimir; Matijasevic, Branimir; and Rusevljan, Miroslav: Generalized Correlations for Heat Transfer Determination in Turbine Cascades. J. Mech. Eng., vol. 47, no. 8, 2001, pp. 468–475.
10. Giel, Paul W., et al.: Heat Transfer Measurements and Predictions on a Power Generation Gas Turbine Blade. ASME 2000–GT–0209 (NASA/TM—2000-210021), 2000. http://ntrs.nasa.gov